Intermodulation Distortion and Power Handling in RF MEMS Switches, Varactors, and Tunable Filters

Laurent Dussopt, *Member, IEEE,* and Gabriel M. Rebeiz, *Fellow, IEEE*

***Abstract*—This paper presents a theoretical and experimental study of the nonlinear effects generated RF-microelectromechanical system (MEMS) varactors and capacitive switches. The theoretical part includes an analytic derivation, as well as an electromechanical model suitable for computer-aided design (CAD) simulation. The simulations agree very well with measurements performed on a 24-GHz three-pole MEMS tunable filter. It is shown that MEMS capacitive components with a spring constant $k > 10$ N/m generate very low intermodulation, as compared to semiconductor devices, and lead to a two-tone third-order intermodulation intercept point (IIP3) greater than $+40$ dBm for $\Delta f > 3$–$5 f_0$, where f_0 is the mechanical resonant frequency. In fact, the IIP3 increases to $+80$ dBm for a difference signal (Δf) of 5 MHz. The CAD model also allows the evaluation of the power-handling capabilities of the tunable filter and, it is seen that, for the case presented here, distortions become significant for an input power greater than $+20$ dBm. Noise generation due to thermal effects on a movable membrane (Brownian noise) is also modeled and it is shown that the tunable filter results in a very low phase-noise level close to the carrier.**

***Index Terms*—Filters, intermodulation (IM), microelectromechanical system (MEMS), microwave, millimeter wave, phase noise, power handling, switches, varactors.**

I. Introduction

MICROELECTROMECHANICAL system (MEMS) switches and varactors have demonstrated impressive performances in terms of losses, reliability, and tuning range during the last few years [1], [2]. Switches have many potential applications in radar and communication systems. Varactors can also be used as tuning elements in filters, phase shifters, or matching networks. Most of these circuits operate at power levels of 1–1000 mW and, therefore, linearity is a critical parameter to prevent distortions or inter-channel interferences.

This paper presents a theoretical and experimental study of nonlinear effects generated by MEMS capacitive switches and varactors. An example of a shunt and series MEMS switch is shown in Fig. 1. The bottom electrode of the switch is covered by a thin dielectric layer in order to create a capacitive contact in the down-state position. MEMS switches are characterized by an up-state capacitance, which varies with the height of the bridge. The beam can be moved using an electrostatic force due to a voltage between the bridge and bottom electrode. This property is used for the actuation of MEMS switches or tuning the capacitance of a varactor. As a consequence, the up-state capacitance is also sensitive to the power of the RF signal, generating nonlinear effects such as intermodulation (IM). However, this paper demonstrates, analytically and experimentally, that these distortions are usually very small and, in many cases, negligible. This is an important advantage of MEMS as compared to other switching components (p-i-n diodes, FET transistors) or tuning elements (varactor diodes, FET transistors, ferroelectric thin films).

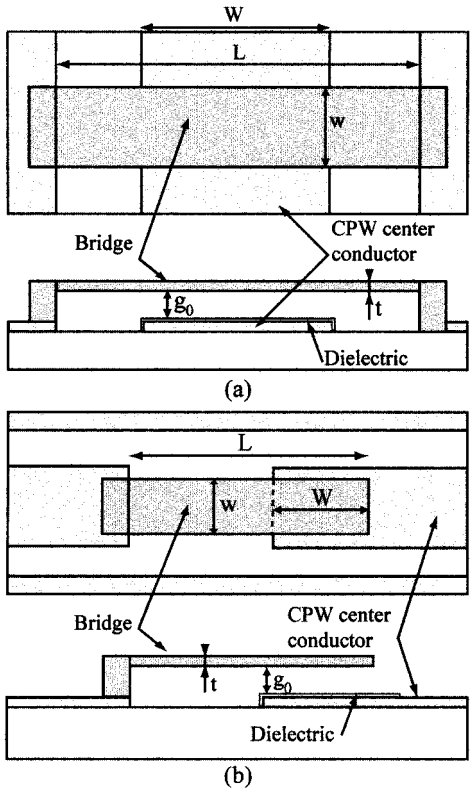

Fig. 1. Top and side views of a: (a) fixed–fixed beam MEMS shunt switch and (b) cantilever series switch.

Manuscript received October 28, 2002; revised November 1, 2002. This work was supported by The University of Michigan at Ann Arbor under a BAE Army Research Laboratory Contract.

L. Dussopt was with the Department of Electrical Engineering and Computer Science, The University of Michigan at Ann Arbor, Ann Arbor, MI 48109-2106 USA. He is now with CEA-LETI, 38054 Grenoble, France (e-mail: Laurent.dussopt@cea.fr).

G. M. Rebeiz is with the Department of Electrical Engineering and Computer Science, The University of Michigan at Ann Arbor, Ann Arbor, Ann Arbor, MI 48109-2106 USA (e-mail: rebeiz@umich.edu).

Digital Object Identifier 10.1109/TMTT.2003.809650

II. Nonlinear Effects in MEMS Capacitive Switches

A. Review of MEMS Electromechanical Modeling

The dynamic mechanical response of a fixed–fixed or cantilever beam is given by the d'Alembert principle and is [3]

$$m\frac{d^2x}{dt^2}+b\frac{dx}{dt}+kx=f_{\text{ext}} \tag{1}$$

where x is the bridge displacement, m is the bridge mass, b is the damping coefficient, k is the spring constant, and f_{ext} is an external force. By using Laplace transforms, the frequency response is

$$\frac{X(j\omega)}{F(j\omega)}=\frac{1}{k}\left(\frac{1}{1-\left(\dfrac{\omega}{\omega_0}\right)^2+\dfrac{j\omega}{(Q\omega_0)}}\right) \tag{2}$$

where $Q=k/(\omega_0 b)$ is the quality factor and $\omega_0=\sqrt{k/m}$ is the resonant frequency. Modal analysis of the beam displacement indicates that only part of the beam actually moves. Consequently, one has to use the effective mass of the beam, which is 0.35×–0.45× the actual mass[1]

$$m_e\approx 0.4\rho Lwt \tag{3}$$

where ρ, L, w, and t are the density, length, width, and thickness of the beam, respectively. The up-state capacitance is $C=C_{\text{pp}}+C_f$, where C_{pp} is the parallel-plate capacitance

$$C_{\text{pp}}=\frac{\epsilon_0 Ww}{g} \tag{4}$$

and C_f is the fringing-field capacitance, which is around 10%–20% of C_{pp} [4]. A voltage applied between the bottom electrode and membrane generates an electrostatic force

$$F=\frac{CV^2}{2g}. \tag{5}$$

For low voltages, the electrostatic force results in a small displacement (Δx) of the membrane and is balanced by the spring restoring force $(F=k\Delta x)$. Increasing the applied voltage increases the displacement Δx until an unstable point where the spring collapses. One can show that the instability occurs for a displacement $\Delta x\approx g_0/3$, where g_0 is the original bridge height, and the corresponding pull-down voltage is

$$V_p=\sqrt{\frac{8kg_0^3}{27\epsilon_0 Ww}}=\sqrt{\frac{8kg_0^2}{27C_0}}. \tag{6}$$

B. Response to a Modulating Signal

An accurate electrical model of a MEMS capacitive switch is shown in Fig. 2 [4]. If we consider the case of the shunt capacitance on a t line and assume that $\omega CZ_0\ll 1$, the transmission coefficient is given by

$$S_{21}=\frac{1}{1+\left(\dfrac{j\omega CZ_0}{2}\right)}\simeq 1-\left(\frac{j\omega CZ_0}{2}\right) \tag{7}$$

[1]MSC Software, Palo Alto, CA.

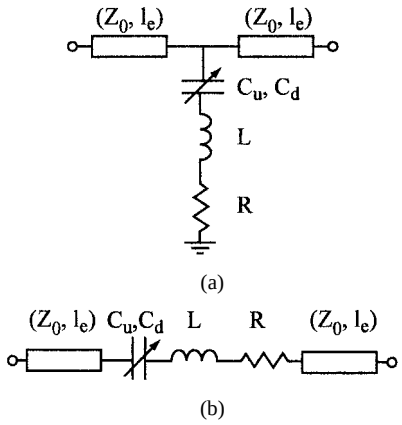

Fig. 2. MEMS switch electrical model. (a) Shunt and (b) series design.

with an output phase and amplitude of

$$\phi\simeq\frac{-\omega CZ_0}{2}\quad |S_{21}|\simeq 1. \tag{8}$$

For a small displacement Δx, the capacitance becomes

$$C(t)=C+\Delta C(t)=\frac{\epsilon_0 Ww}{g+\Delta x(t)}+C_f\simeq C\left(1-\frac{\Delta x(t)}{g}\right). \tag{9}$$

Inserting this expression in (8) results in

$$\phi+\Delta\phi(t)=\phi\left(1-\frac{\Delta x(t)}{g}\right). \tag{10}$$

It is seen that a small displacement results in a capacitance change and, therefore, a phase modulation of the output voltage. The output spectrum, in turn, will include several sidebands at $\omega\pm n\omega_m$ if Δx is varying at a frequency ω_m.

Consider the case of an incident signal including three components: bias (dc), a low-frequency modulating signal at ω_m, and an RF signal at ω

$$V=V_{\text{bias}}+V_m\sin(\omega_m t)+V_{\text{RF}}\sin(\omega t). \tag{11}$$

Assuming that $\omega_m\lesssim\omega_0$ and $\Delta x\ll g$, the displacement is

$$\Delta x(t)\simeq\frac{F}{k}\simeq\frac{C}{2kg}\left\{V_{\text{bias}}^2+\frac{V_m^2}{2}+\frac{V_{\text{RF}}^2}{2}+2V_{\text{bias}}V_m\sin(\omega_m t)-\frac{V_m^2}{2}\cos(2\omega_m t)\right\} \tag{12}$$

where the high-frequency terms at ω, 2ω, and $\omega\pm\omega_m$ are neglected since $\omega\gg\omega_0$. Using (8) and (10), the RF output signal becomes

$$\begin{aligned}V_0=&V_{\text{RF}}\sin\left(\omega t+\phi+\Delta\phi(t)\right)\\ \simeq&V_{\text{RF}}\sin(\omega t+\phi)\\ &\mp V_{\text{bias}}V_m V_{\text{RF}}\frac{\phi C}{2kg^2}\sin\left((\omega\pm\omega_m)t+\phi\right)\\ &+\frac{V_m^2 V_{\text{RF}}}{4}\frac{\phi C}{2kg^2}\cos\left((\omega\pm 2\omega_m)t+\phi\right)\end{aligned} \tag{13}$$

where $\phi=-(\omega CZ_0)/2$. Notice that if there is no dc bias $(V_{\text{bias}}=0)$, the modulation components at $\omega\pm\omega_m$ are null and the sidebands occur only at $\omega\pm 2\omega_m$. Also, the sidebands

TABLE I
SWITCH/VARACTOR MODEL PARAMETERS

C_0 (fF) ($A = 160$x210 μm^2)	100
g_0 (μm)	3
Spring constant (N/m)	k=10
Mechanical Q	Q=1.7
f_0 (kHz)	60

at $\omega \pm 2\omega_m$ are indirectly dependent on $V_{\rm bias}$ through the bridge height g. The modulation level at $\omega \pm \omega_m$ is

$$P_{{\rm mod},\omega_m} = \frac{P_{\rm sideband}}{P_{\rm signal}} = \left(V_{\rm bias} V_m \frac{\phi C}{2kg^2}\right)^2. \quad (14)$$

There are also two modulation components at $\omega \pm 2\omega_m$

$$P_{{\rm mod},2\omega_m} = \frac{P_{\rm sideband}}{P_{\rm signal}} = \left(\frac{V_m^2}{4}\frac{\phi C}{2kg^2}\right)^2. \quad (15)$$

The modulation level follows the low-pass response of (2), and it is easy to prove that, if $\omega_m = \omega_0$ or $\omega_m \gg \omega_0$, then the modulation levels derived in (14) and (15) are multiplied by Q^2 and $(\omega_0/\omega_m)^4$, respectively. Also, $P_{\rm mod}$ varies as ω^2 and C^4 and, therefore, the modulation effect is more important in varactors (which have a higher C than switches) and at high RF frequencies.

An RF-MEMS switch with the parameters indicated in Table I and $Z_0 = 50\,\Omega$ at 10 GHz with $V_{\rm bias} = 0$ V (up-state) and $V_m = 3$ V results in a modulation component at $2\omega_m$ of -74.1 dBc. The pull-down voltage is 16.3 V (6). If a bias voltage $V_{\rm bias} = 10$ V is applied, the bridge height and capacitance can be estimated from (5), (1), and (4) and are $g = 2.83$ μm and $C = 106$ fF, respectively. The modulations levels are then -48.1 dBc and -70.6 dBc at $\omega \pm \omega_m$ and $\omega \pm 2\omega_m$, respectively.

C. Response to Multiple Signals: IM

Consider the case of two incident signals on a t line ($V_i = V_1 \sin(\omega_1 t) + V_2 \sin(\omega_2 t)$). The output signal is

$$V_0 \simeq V_{\rm bias} + V_1 \sin(\omega_1 t + \phi) + V_2 \sin(\omega_2 t + \phi). \quad (16)$$

Assuming that $\omega_1 - \omega_2 \ll \omega_0$, the displacement is

$$\Delta x(t) \simeq \frac{F}{\rm k} \simeq \frac{C}{2kg}\left\{V_{\rm bias}^2 + \frac{V_1^2}{2} + \frac{V_2^2}{2} + 2V_1V_2\cos\left((\omega_1 - \omega_2)t\right)\right\} \quad (17)$$

where the high-frequency terms at ω_1, ω_2, $2\omega_1$, $2\omega_2$, and $\omega_1 + \omega_2$ are neglected since $\omega_{1,2} \gg \omega_0$. Using (8) and (10), the RF output signal becomes

$$\begin{aligned} V_0 =& V_1 \sin\left(\omega_1 t + \phi + \Delta\phi(t)\right) \\ &+ V_2 \sin\left(\omega_2 t + \phi + \Delta\phi(t)\right) \\ \simeq& V_1 \sin(\omega_1 t + \phi) + V_2 \sin(\omega_2 t + \phi) \\ &- \frac{V_1 V_2}{2}\frac{\phi C}{2kg^2} \\ &\times \left\{V_1 \cos\left((2\omega_1 - \omega_2)t + \phi\right)\right. \\ &\left. + V_2 \cos\left((2\omega_2 - \omega_1)t + \phi\right)\right\}. \end{aligned} \quad (18)$$

Assuming $V_1 = V_2$, the IM products level at $2f_1 - f_2$ and $2f_2 - f_1$ is

$$P_{\rm intermod} = \frac{P_{\rm sideband}}{P_{\rm signal}} = \left(V_1 V_2 \frac{\phi}{2}\frac{C}{2kg^2}\right)^2 \quad (19)$$

where g depends on the bias voltage. Notice that the IM components always occur at $2f_2 - f_1$ and $2f_1 - f_2$ independently of the bias voltage. The two-tone third-order intermodulation intercept point (IIP3) corresponds to the value of $P_{\rm signal}$, for which $P_{\rm signal} = P_{\rm sideband}$, and can be easily derived from (19)

$$\text{IIP3} = \frac{2kg^2}{\phi C Z_0}. \quad (20)$$

For the RF-MEMS switch considered above, and with $V_1 = V_2 = 3.16$ V ($P_1 = P_2 = 100$ mW) at 10 GHz, the resulting IM level is -67.2 dBc, and the corresponding IIP3 is $+55.1$ dBm.

As in the modulation case, the IM power depends on ω^2 and C^4 and, therefore, the IM products are much larger for MEMS varactors than for MEMS switches and at high RF frequencies. The IM power level is extremely sensitive to g and varies as $1/g^8$ for a constant varactor area. This is due to the C^4 and $1/g^4$ terms in (14), (15), and (19). Finally, $P_{\rm intermod}$ varies as k^{-2}, and low spring-constant varactors can generate relatively high IM levels.

Thus far, we have discussed the IM products in the transmitted signal, but the reflected wave has the same IM products relative to the carrier since the reflection coefficient is

$$S_{11} = \frac{-j\omega C Z_0}{2 + j\omega C Z_0} \simeq \frac{-j\omega C Z_0}{2}. \quad (21)$$

Since the reflected signal from a shunt switch in the up-state is quite low, the IM generated will be very low as well and should not be significant.

A similar analysis can be done for a capacitive series switch with

$$\begin{aligned} S_{11} =& \frac{1}{1 + 2j\omega C Z_0} \simeq 1 - 2j\omega C Z_0 \\ S_{21} =& \frac{2j\omega C Z_0}{1 + 2j\omega C Z_0}. \end{aligned} \quad (22)$$

In this case, it is the reflected wave, which is very high when the switch is in the up-state position. The series capacitive switches result in 4 $\times$ more phase variation and, therefore, 16 $\times$ more IM products as compared to shunt capacitive switches for the *same* up-state capacitance. This is expected since the RF voltage on a series capacitive switch in the up-state position (open circuit) is twice that of a shunt capacitive switch.

For series and shunt capacitive switches, in the down-state position, the IM products depend only on the dielectric linearity and are very low. In the case of metal-contact switches, the IM generated is extremely low because of the very small capacitance in the up-state position (2–10 fF) and the low nonlinearities of the metal–metal contact in the down-state position.

The calculations presented in this section assumed that the switch impedance is high ($\omega C Z_0 \ll 1$) to justify the approximations of (7) and (8). However, in the case of a varactor, the capacitance can be quite large and an analytic derivation of the modulation or IM levels would involve more complicated expressions. Another approach is to use a computer-aided

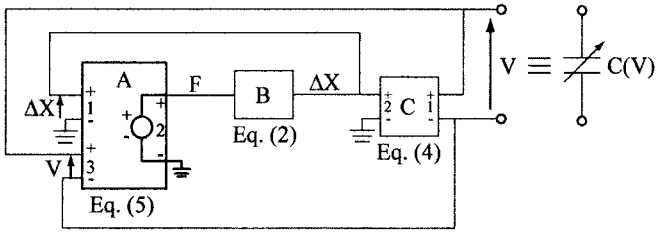

Fig. 3. Nonlinear CAD model of a MEMS capacitive switch or varactor in the up-state position.

design (CAD) electromechanical model, as presented in Section III, which, in addition, permits to simulate complex circuits including several MEMS devices.

III. CAD Electromechanical Model of a MEMS Beam

In order to study the IM generation in circuits using MEMS switches or varactors, a nonlinear model of the MEMS device in the up state has been implemented in Agilent ADS[2] (Fig. 3). A nonlinear mechanical model of a MEMS switch using mechanical/electrical equivalencies has already been presented by Mercier *et al.* [6]. The present model implements directly (1), (5), and (9) and seems more straightforward. However, the authors believe that both models should provide similar capabilities for the analysis presented in this paper. The module C is the capacitance model with a port-1 impedance $Z = 1/j\omega C$. In this equation, the value of C is calculated from (4) using the displacement of the membrane Δx, which is represented by an equivalent voltage at port 2. The membrane displacement Δx is calculated from the electrostatic force by module B, which uses (2). This relation is actually the transfer function of a second-order low-pass filter and its implementation is straightforward using the polynomial low-pass filter module of *ADS*. The electrostatic force is calculated by module A from the voltage V (port 3) and the displacement Δx (port 1). This module generates an output voltage F equivalent to the electrostatic force (5).

We present in this section some simulation results of a MEMS shunt switch showing the basic response of the device to the bias voltage or the RF signal. The switch is identical to the device considered in Section II and its characteristics are listed in Table I.

Fig. 4 shows the height and capacitance of the bridge for a bias voltage of $0 - V_p$ for the MEMS switch of Table I. The displacement of the membrane at $V = 16$ V is 0.78 μm, and the parallel-plate capacitance ratio is 1 : 1.35. Fig. 5 presents the membrane displacement versus time for a sinusoidal modulation ($V_m = 3$ V) at a frequency of $f_m = 1$, 30, and 100 kHz ($V_{\text{bias}} = 0$ V). As shown in (13), the component at f_m is null since $V_{\text{bias}} = 0$ V and the modulation occurs at $2f_m$. The membrane position waveforms are also at twice the modulating frequency and, therefore, the maximum displacement occurs for $f_m = 30$ kHz, which is half the mechanical resonance. At low modulating frequency, the membrane follows the bias waveform, while at 100 kHz, the variations of the electrostatic force are greatly attenuated by the low-pass mechanical characteristic

[2]*ADS 2002*, Agilent Technol. Inc., Palo Alto, CA

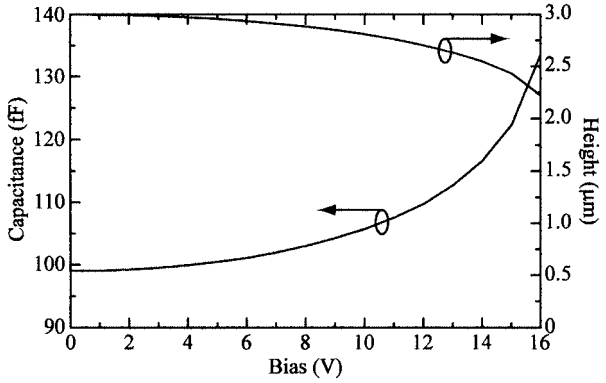

Fig. 4. MEMS varactor: parallel-plate capacitance and bridge height versus bias calculated with *ADS* model.

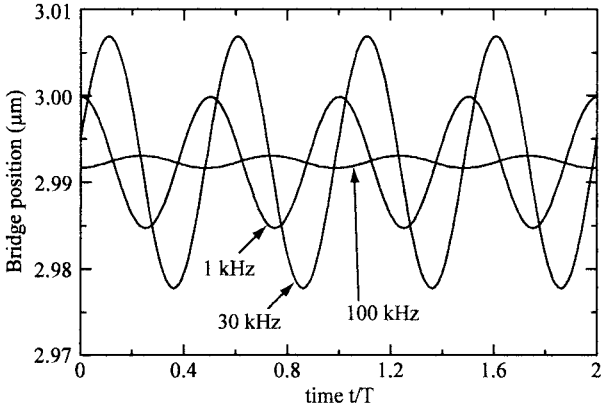

Fig. 5. Modulation of an RF carrier ($f = 10$ GHz, $P = 0$ dBm) by a low frequency ($f_m = 1$, 30, and 100 kHz) sinusoidal voltage ($V_m = 3$ V): bridge position versus time (time scale is normalized to the period of the low-frequency signal).

of (2) and the membrane shows small oscillations around an average value of 2.993 μm. The output spectrum is shown in Fig. 6(a) for an incident RF signal at 10 and 24 GHz, and for a dc bias of 0 and 10 V. The modulation levels simulated at 10 GHz with $V_{\text{bias}} = 0$ V confirm the calculations made in Section II-B. Fig. 6(b) shows the modulation level versus modulation frequency f_m. This plot is similar to the mechanical characteristic of (2), but with a resonance frequency of $f_0/2$ if $V_{\text{bias}} = 0$ V and f_0 if $V_{\text{bias}} \neq 0$ V. The modulation level also drops as $(\omega_0/\omega_m)^4$ for $\omega_m > \omega_0$. This shows that a varactor or a switch does not generate any significant level of modulation components for bias variations or parasitic signals above 3–5 f_0.

Fig. 7 shows the force and displacement waveforms calculated with the nonlinear circuit model assuming two incoming waves at frequencies f_1 and f_2, and the resulting IM level is shown in Fig. 8 for an RF power of 10–1000 mW. Again, the IM simulated for $P_{\text{in}} = 100$ mW agrees well with calculation of Section II-C. The IIP3 is minimum at $\Delta f = f_0$ and is +51 dBm. The IM-to-carrier ratio increase from $P_{\text{in}} = 10$ mW to $P_{\text{in}} = 100$ mW is approximately 20 dB, which agrees with (19). From $P_{\text{in}} = 100$ mW to $P_{\text{in}} = 1000$ mW, this level increases by 24.6 dB because of the self-biasing effect of the high-power RF signal, which lowers the membrane height.

The IIP3 of a single varactor is shown in Fig. 9 as a function of the spring constant k and for several bridge height g. The

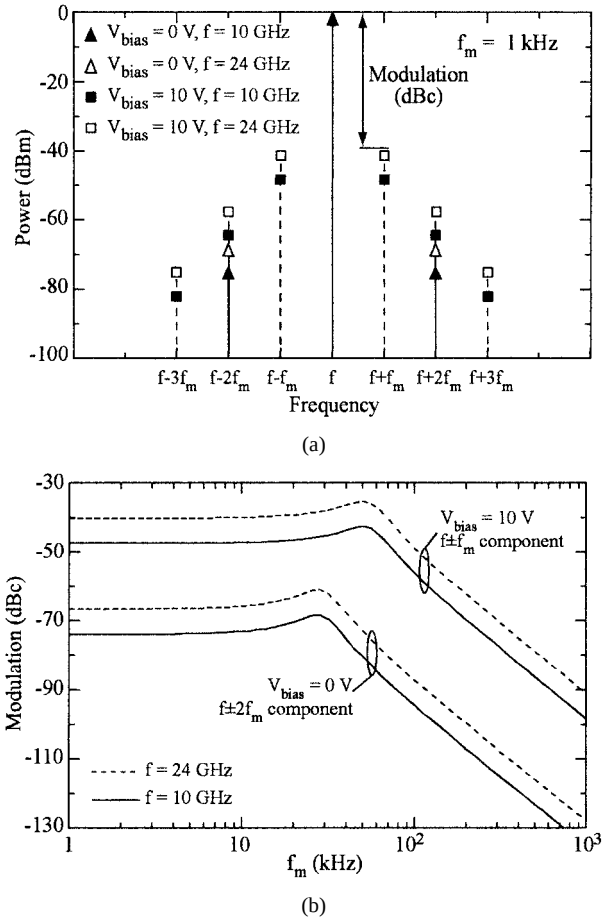

Fig. 6. Modulation of an RF carrier ($f = 10$ and 24 GHz, $P = 0$ dBm) by a low-frequency (f_m) sinusoidal voltage ($V_m = 3$ V). (a) Output spectrum at $f_m = 1$ kHz and (b) modulation level versus f_m (see Table I for details).

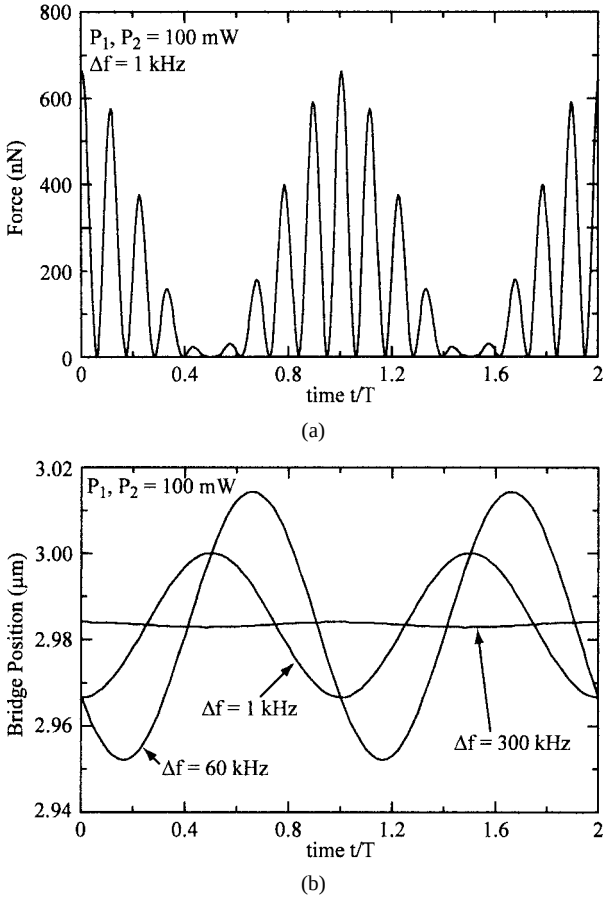

Fig. 7. IM between two RF signals ($P = 100$ mW, $f_1 = 10$ GHz). (a) Electrostatic force and (b) bridge position versus time (see Table I for details).

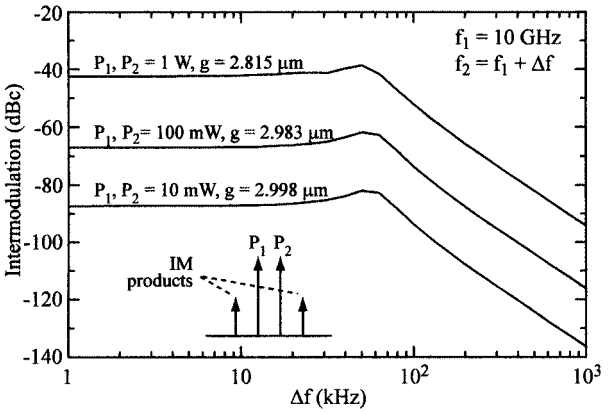

Fig. 8. Two-tone IM-to-carrier ratio at 10 GHz for $P_{\text{in}} = 10, 100$, and 1000 mW (see Table I for details).

parallel-plate area is $A = 140 \times 140\ \mu\text{m}^2$ corresponding to a capacitance $C = 87$ fF for $g = 2\ \mu$m. As expected from (20), the IIP3 increases by 10 dB/decade with k and by 12 dB when g is doubled (varies as g^4). This simulation of IIP3 agrees within ± 0.2 dB with the analytical derivation of Section II (20). These results show that, for a spring constant $k > 10$ N/m and a gap $g > 2\ \mu$m, the IIP3 of this varactor ($A = 140 \times 140\ \mu\text{m}^2$) is greater than +50 dBm. The characteristics of a different varactor can be easily deduced from this graph since the IIP3 varies as A^{-2} and f^{-1} (20).

The IM levels are so low that it is very hard to measure them using a single MEMS switch or varactor. However, if the MEMS varactor is placed in a resonator or a filter, it experiences much higher RF voltages and generates measurable quantities of IM products. This is done in Section IV.

IV. IM Generation in a 24-GHz Tunable Filter

A 24-GHz three-pole 7% tunable filter has been previously developed by Abbaspour-Tamijani *et al.* [5] (Fig. 10). The circuit is built on quartz ($\epsilon_r = 3.8$). The measured 1-dB bandwidth is 6.6%–8.4% with a 5.1% tuning range (22.6–23.8 GHz). The insertion loss is from −2.8 to −3.8 dB and the return loss is better than −12 dB over the entire tuning range (Fig. 11). This filter uses six MEMS varactors whose parameters are given in Table II.

The voltage at each varactor is given in Fig. 12 as a function of frequency for an input power of 10 mW. It is seen that, due to the resonant structure of the circuit (each resonator has a Q of around 50–60), the voltage can go up to 2 V, which is much more than in the case of a switch on a t line, where the voltage is ∼0.7 V for the same incident power. Consequently, the IM generation is more important in this circuit as compared to a standard varactor across a t line.

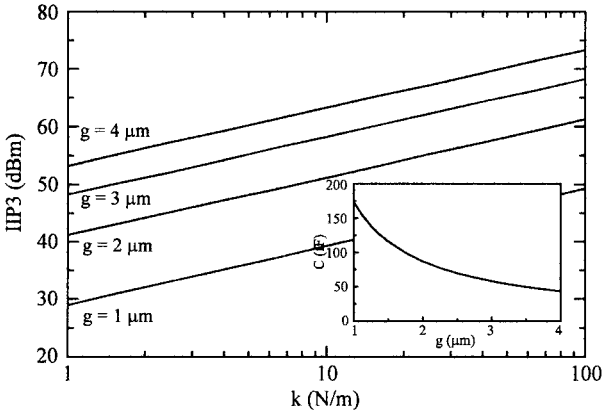

Fig. 9. IIP3 of a single varactor as a function of the spring constant for several membrane heights ($f = 10$ GHz, $\Delta f = 10$ kHz), and the corresponding parallel-plate capacitance versus g ($A = 140 \times 140\ \mu\text{m}^2$).

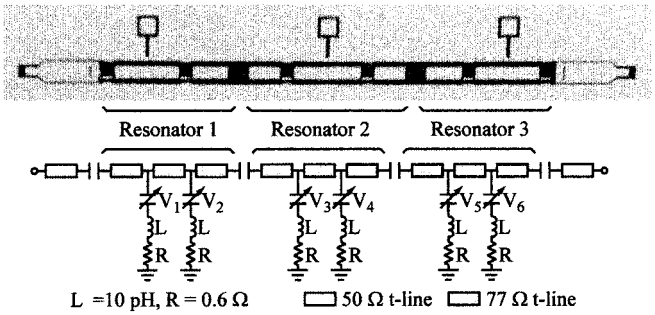

Fig. 10. 24-GHz three-pole 7% tunable filter. (a) Photograph. (b) Model.

Fig. 13 presents the IM measurement setup. The two signals are combined through a 10-dB coupler, which is preceded by two isolators to reduce the residual IM generated by the amplifiers. Measurements are done on wafer and the output spectrum is measured with an HP 8564E spectrum analyzer. Fig. 13(b) presents the output spectrum of the filter for $P_{\text{in}} = 10$ mW and $\Delta f = 60$ kHz.

The IM products have been measured for $P_1 = P_2 = -1$ to $+10$ dBm, $\Delta f = 5$–500 kHz, $f = 24$ GHz and no bias voltage on the varactors [see Fig. 14(a)]. The noise floor and residual IM of the measurement setup limited our experiment to $\Delta f < 400$–500 kHz. The measurements agree very well with the simulation and confirm the -40 dB/decade decrease rate of the IM for $\Delta f > f_0$. The simulation is done by inserting the nonlinear model of Fig. 3 for each MEMS varactor in the filter of Fig. 10 and doing a standard two-tone harmonic-balance simulation. From these measurements, one can plot the output and IM power versus input power and deduce the IIP3 [see Fig. 14(b)]. As expected, the IIP3 is minimum at the resonant frequency of the bridges $(+26.6$ dBm$)$, but increases to $+39$ dBm at 200 kHz and $+42$ dBm at 500 kHz. These results demonstrate that MEMS tunable filters do not generate any significant IM product for signals separated by over 500 kHz, as is the case in most multichannel communication systems (inter-channel interference).

For completeness, the IM has been measured versus frequency and for several bias voltages (Fig. 15). Effectively, as

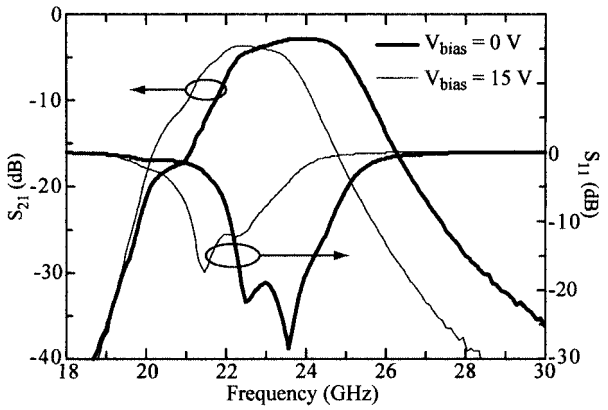

Fig. 11. Measured S-parameters of the 24-GHz three-pole 7% tunable filter for $V_{\text{bias}} = 0$ V and 15 V.

TABLE II
VARACTOR MODEL PARAMETERS FOR THE 24-GHZ TUNABLE FILTER

Membrane dimensions (μm)	l, w, t = 300, 130, 1.2
C_0 (fF) ($A = 130$x$160\ \mu\text{m}^2$)	142
g_0 (μm)	1.4
Metal	gold
Spring constant (N/m)	k=55
Mechanical Q	Q=1.7
f_0 (kHz)	60

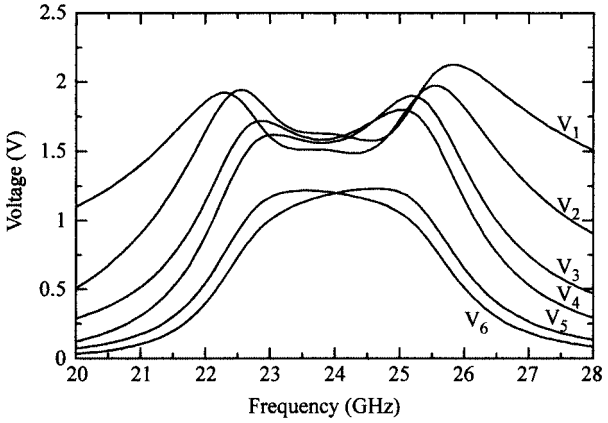

Fig. 12. Simulated peak RF voltage at each MEMS varactor ($V_1 - V_6$) of the 24-GHz tunable filter ($P_{\text{in}} = 10$ dBm).

shown in Fig. 12, the voltage at each varactor depends on the frequency and, thus, do the IM products. Again, we observe a fairly good agreement between measurements and simulations. The IM products are 4–6 dB higher at each edge of the passband than in the middle, which means a 2–3 dB lower IIP3.

The dependence of the IM products versus varactor bias at 24 GHz was simulated (Fig. 15). An increase of roughly 12 dB is observed at the maximum bias. This result agrees well with the measurements shown in Fig. 15 and the theory. Effectively, (8) and (19) show that the IM products depend on $1/g^8$, and assuming that the bridge height is reduced by 30% at $V_{\text{bias}} = 14$ V, the IM level should be increased by a factor $10\log(1/0.7^8) = 12.4$ dB.

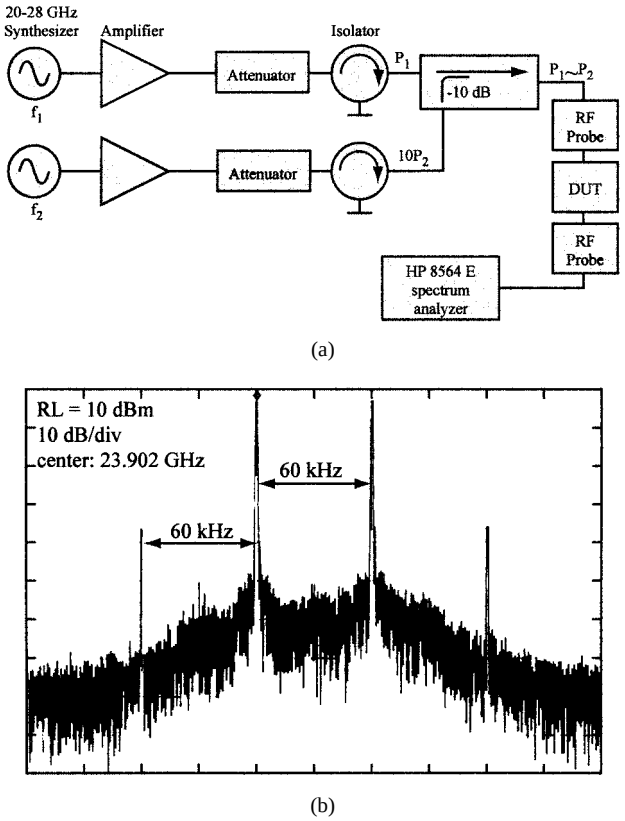

(a)

(b)

Fig. 13. (a) IM measurement setup. (b) Output spectrum for $P_1 = P_2 = 10$ mW and $\Delta f = 60$ kHz.

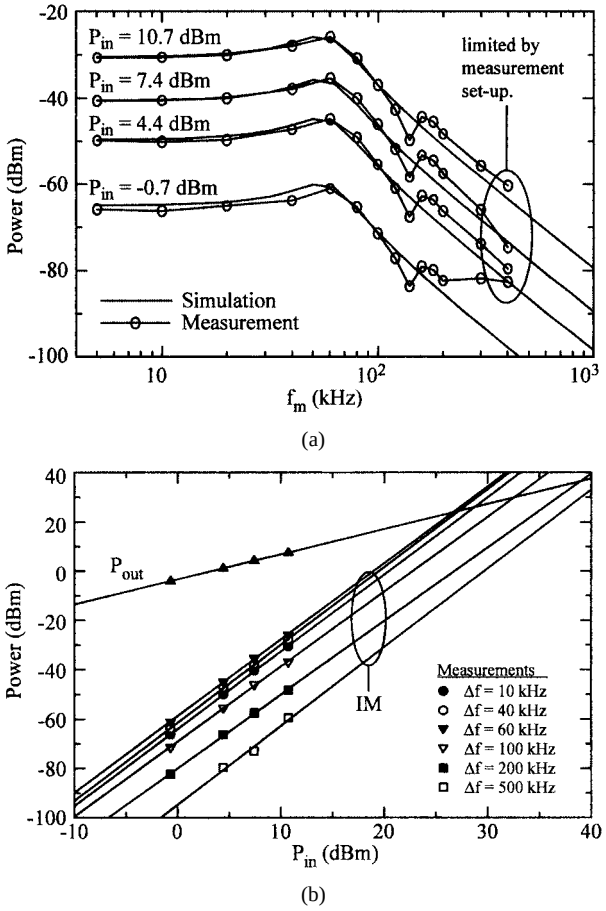

(a)

(b)

Fig. 14. Filter IM products measurements. (a) IM level versus Δf. (b) IM level versus input power ($f = 24$ GHz, $V_{\rm bias} = 0$ V).

V. Power Handling of a 24-GHz Tunable Filter

Power handling and self-biasing of MEMS devices is more critical for MEMS varactors than for switches since the parallel-plate area is usually quite large and the membrane height determines the capacitance value. The self-biasing of single switches or varactors has been investigated by Muldavin [8] and Mercier *et al.* [7]. A membrane pulls down by self-actuation when the RF rms voltage is equal to the dc pull-down voltage, and this occurs at $P_{\rm RF} = 3.9$ W for the varactor of Table II (pull-down voltage $V_p = 14$ V). It is, therefore, important to simulate MEMS-tunable filters under high RF power conditions since a small input power can generate fairly large voltages across the MEMS varactors (see Fig. 12). Fig. 16(a) shows the simulated large-signal S-parameters of the 24-GHz filter for several input power values from 0 to 28 dBm. It is seen that there is no significant variation in the S-parameters for $P_{\rm in} \leq +20$ dBm. This is confirmed by the measurements of Fig. 16(b). However, simulations for $P_{\rm in} = +26$ and $+28$ dBm indicate a significant self-biasing of the varactors, with peak RF voltage values up to 17–20 V. For $P_{\rm in} > +28$ dBm, the harmonic-balance simulation does not converge, which indicates that at least one bridge is pulled down as the rms RF voltage across the varactors reaches the pull-down voltage (14 V).

Another self-biasing effect of practical interest is the *passive IM* generated when the filter is fed with an amplitude-modulated RF signal at 24 GHz. We have simulated the filter fed by a pulsed source with $P_{\rm in} = 0$-$20, 0$,–23, and 0–26 dBm [see Fig. 17(a)]. The magnitude and phase of S_{21} are shown

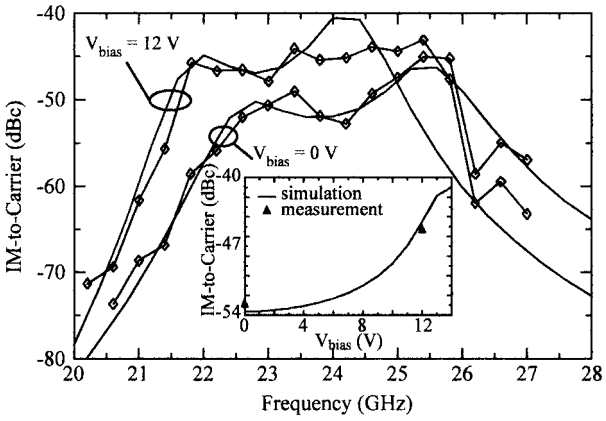

Fig. 15. IM-to-carrier ratio versus frequency (—— simulation, —◇— measurement). Insert: IM-to-carrier ratio versus varactor bias at $f = 24$ GHz ($\Delta f = 20$ kHz, $P_{\rm in} = 5$ dBm).

in Fig. 17(b) for a pulse rate of 20 kHz. As expected, significant amplitude and phase deviations occur for a peak power greater than 20 dBm. Fig. 18 shows the spectrum of the input signal for $P_{\rm in} = 0$–23 dBm and the output spectrum for $P_{\rm in} = 0$–$20, 0$–23, and 0–26 dBm. The nonlinearities of the filter generate strong additional spectral components at ± 40 kHz, ± 80 kHz, ± 120 kHz, etc. as a result of IM between

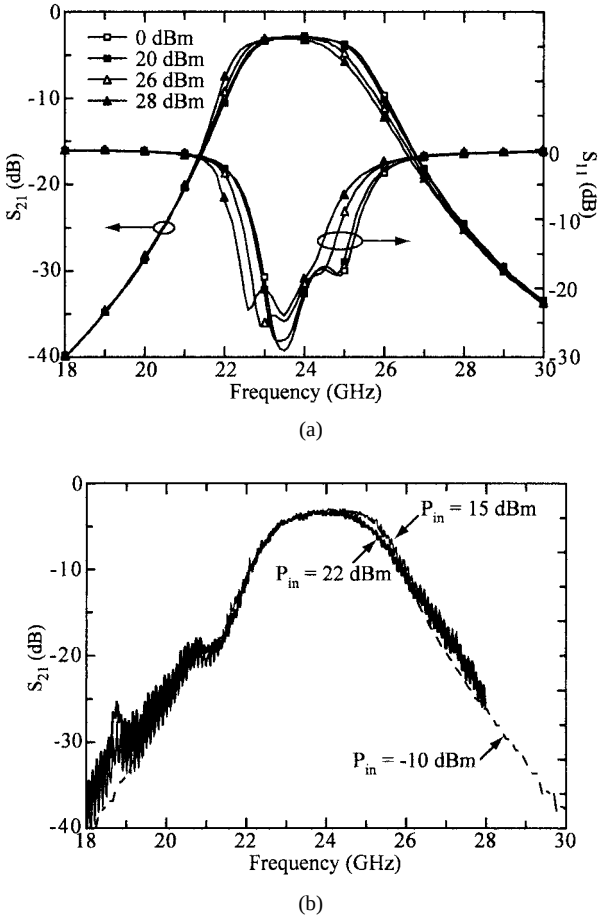

Fig. 16. (a) Simulated large-signal S-parameters of the 24-GHz three-pole tunable filter for $P_{\rm in} = 0, 20, 26,$ and 28 dBm. (b) Measured S-parameters for $P_{\rm in} = -10, 15,$ and 23 dBm ($V_{\rm bias} = 0$ V).

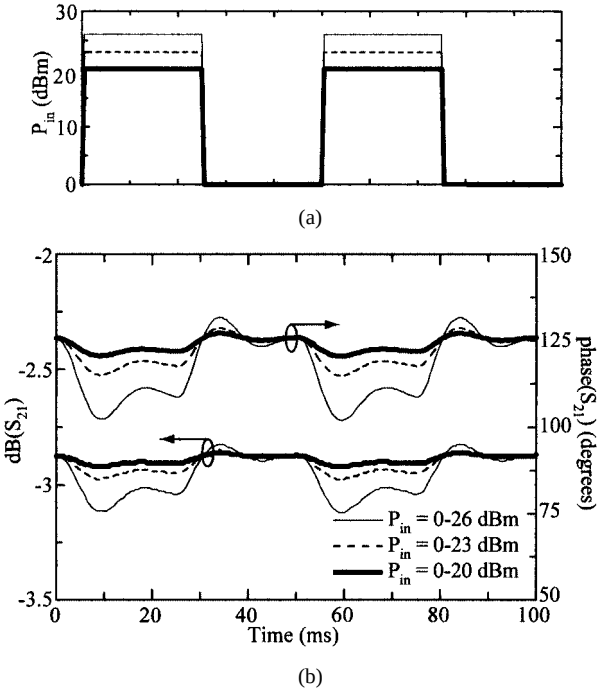

Fig. 17. Simulated passive IM in the tunable filter at 24 GHz for a pulsed input signal with $P_{\rm in} = 0{-}20, 0{-}23,$ and $0{-}26$ dBm. (a) Envelope of the input signal versus time. (b) Magnitude and phase of the transmission coefficient versus time (pulse rate: 20 kHz).

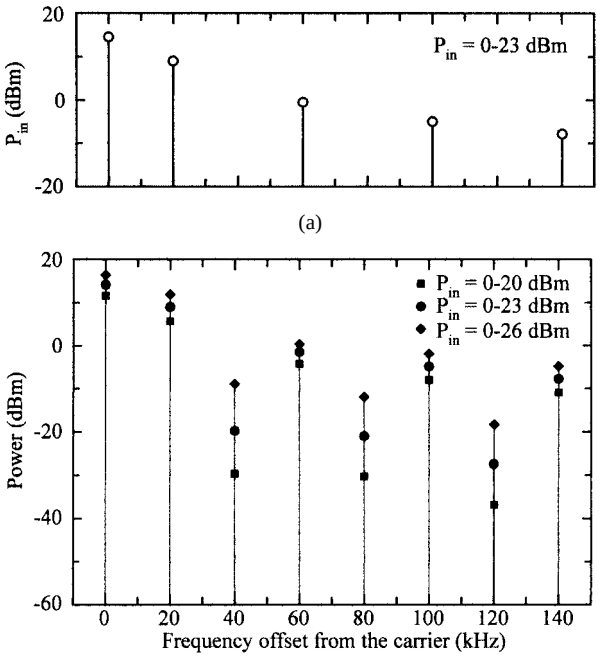

Fig. 18. Simulated passive IM in the tunable filter at 24 GHz for a pulsed input signal. (a) Spectrum of the input signal ($P_{\rm in} = 0{-}23$ dBm). (b) Output spectrum ($P_{\rm in} = 0{-}23, 0{-}23,$ and $0{-}26$ dBm) (pulse rate: 20 kHz).

the carrier and modulating signal. As in the case of the two-tone IM, the distortions generated are maximum at the resonant frequency of the membrane ($f_0 = 60$ kHz) and become negligible for pulse rates greater than 200–300 kHz (3–5 f_0).

This section shows that the practical power handling of the filter presented is roughly +20 dBm. A higher power handling can be obtained with a higher spring constant: the pull-down voltage varies as $\sqrt{k}$ and, therefore, the maximum allowable RF power varies as k. A high spring constant benefits to the filter also in terms of IIP3 (Section III), and in terms of noise, as is shown in Section VI.

VI. Phase-Noise Generation

Thermal noise (or Brownian noise) generates a mechanical force on the membrane given by $f_n = \sqrt{4k_BTb}$ (in $N/\sqrt{Hz}$), where k_B is the Boltzman constant, T is the temperature, and b is the damping coefficient [9]. This effect can be taken into account in the model of Fig. 3 by including a noise voltage source in series between blocks A and B with an rms voltage of $v_n = f_n$ (in $V/\sqrt{Hz}$). The random displacement of the membrane x_n is equal to the noise force f_n multiplied by the transfer function of (2), and results in a random phase and amplitude variation at the output of the MEMS switch or varactor.

The phase noise generated by the Brownian noise for a shunt switch or varactor is [9]

$$P_{\rm ph} = \frac{1}{2}\frac{1}{(1+\gamma)^2}\frac{\overline{x_n^2}}{g^2}\phi^2 \ {\rm Hz}^{-1} \tag{23}$$

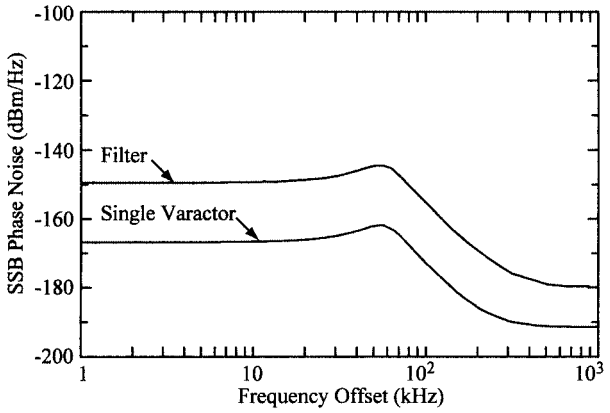

Fig. 19. Simulated phase noise generated in a single varactor and in the 24-GHz three-pole tunable filter for a 0-dBm input signal at 24 GHz.

where γ is the ratio of the fringing capacitance to the parallel-plate capacitance ($\gamma = C_f/C_{\rm pp}$), and $\phi = \omega C Z_0/2$ is the phase delay due to the MEMS component. In (23), x_n varies as $1/k$ and, therefore, low spring constant devices generate higher phase noise close to the carrier. For the varactor of Table II with $\gamma = 0.08$ and for $f = 24$ GHz, $T = 290$ K, the phase noise relative to the carrier calculated using (23) is $P_{\rm ph} = -165.5$ dBc/Hz. This agrees well with the simulated results of Fig. 19 for an offset frequency of dc–60 kHz (dc–f_0). For offset frequencies larger than the mechanical resonance, the phase noise decreases at a rate of -40 dB/decade and is eventually limited by the MEMS varactor series resistance noise (-191 dBm/Hz, $R_s = 0.6\,\Omega$) since there is no loss in the t line. The 24-GHz tunable filter has been simulated using the circuit of Fig. 10(b) and the noise model presented above, and results in an output phase noise level of -146.2 dBc/Hz close to the carrier and -180 dBc/Hz at high offset frequencies, limited by the 3-dB loss in the filter (Fig. 19).

The amplitude noise generated by the Brownian noise in MEMS switches is [9]

$$P_{\rm am} = \frac{1}{2}\frac{1}{(1+\gamma)^2}\frac{\overline{x_n^2}}{g^2}\phi^4\ {\rm Hz}^{-1} \tag{24}$$

and, for the case of the MEMS varactor of Table II at 24 GHz, ($C_u = 142$ fF), (24) ($P_{\rm am} = -171$ dBm/Hz) agrees quite well with the nonlinear circuit model of Fig. 3 ($P_{\rm am} = -169$ dBm/Hz).

It is worth noting that, comparing (23) and (24), the phase and amplitude noise components are related by $P_{\rm am} = P_{\rm ph}\phi^2$. For a MEMS *switch* with $C_u = 50$ fF at 10 GHz ($\phi = 0.078$ rad), the amplitude noise is 22 dB lower than the phase noise due to the much smaller capacitance and ϕ. However, for the MEMS *varactor* with $C_u = 142$ fF at 24 GHz ($\phi = 0.535$ rad), the two noise components are within 5.4 dB due to the much larger capacitance of the MEMS device.

VII. Conclusion

This paper has shown that MEMS varactors do not move at difference signal frequencies Δf greater than 200 kHz and, therefore, generate very low IM products. This makes RF MEMS switches and varactors very attractive for tunable filters, matching networks, or phase-shifter applications in communication systems.

A complete CAD model was also developed, which allows the user the capability to predict the IM levels, power handling, and Brownian noise generation of MEMS varactors and tunable filters and networks. For the 24-GHz three-pole 7% filter, an input power up to 20 dBm does not generate any significant distortion of the filter response due to self-biasing or passive IM. The phase noise generated in the filter is of the order of -147 dBc/Hz close to the carrier, but falls off to insignificant levels at offset frequencies greater than 3–5 f_0.

References

[1] G. M. Rebeiz and J. B. Muldavin, "RF MEMS switches and switch circuits," *IEEE Microwave Mag.*, vol. 2, pp. 59–71, Dec. 2001.

[2] G. M. Rebeiz, G.-L. Tan, and J. S. Hayden, "RF MEMS phase shifters: Design and applications," *IEEE Microwave Mag.*, vol. 3, pp. 72–81, June 2002.

[3] W. Weaver, Jr., S. P. Timoshenko, and D. H. Young, *Vibration Problems in Engineering*, 5th ed. New York: Wiley, 1990.

[4] J. B. Muldavin and G. M. Rebeiz, "High-isolation MEMS shunt switches—Part 1: Modeling," *IEEE Trans. Microwave Theory Tech.*, vol. 48, pp. 1045–1052, June 2000.

[5] A. Abbaspour-Tamijani, L. Dussopt, and G. M. Rebeiz, "A millimeter-wave tunable filter using MEMS capacitors," in *32nd Eur. Microwave Conf.*, Milan, Italy, Sept. 2002, pp. 813–815.

[6] D. Mercier, P. Blondy, D. Cros, and P. Guillon, "An electromechanical model for MEMS switches," in *IEEE Int. Microwave Theory Tech. Symp.*, Phoenix, AZ, June 2001, pp. 2123–2126.

[7] D. Mercier, P. Blondy, D. Barataud, D. Cros, P. Guillon, C. Champeaux, P. Tristant, and A. Catherinot, "Model for MEMS switches power handling and phase noise," in *32nd Eur. Microwave Conf.*, Milan, Italy, Sept. 2002, pp. 219–222.

[8] J. B. Muldavin, "Design and analysis of series and shunt MEMS switches," Ph.D. dissertation, Dept. Elect. Eng. Comput. Sci., The Univ. Michigan at Ann Arbor, Ann Arbor, MI, 2001.

[9] G. M. Rebeiz, "Phase noise analysis of MEMS-based circuits and phase shifters," *IEEE Trans. Microwave Theory Tech.*, vol. 50, pp. 1316–1323, May 2002.

Laurent Dussopt (S'00–A'01–M'03) received the M.S. and Agrégation degrees in electrical engineering from the Ecole Normale Supérieure de Cachan, Cachan, France, in 1994 and 1995, respectively, and the Ph.D. degree in electrical engineering from the University of Nice-Sophia Antipolis, Nice-Sophia Antipolis, France, in 2000.

From September 2000 to October 2002, he was a Research Fellow with The University of Michigan at Ann Arbor, where he was involved with RF-MEMS varactors and switches and their applications to voltage-controlled oscillators (VCOs), phase shifters, and tunable networks. He is currently with CEA-LETI, Grenoble, France. He has authored or coauthored over 25 journal and conference papers and several book chapters. His research interests include RF-MEMS components and systems, planar antennas and arrays, active antennas, and oscillating antenna arrays.

Dr. Dussopt has been a reviewer of several papers for the IEEE Transactions on Microwave Theory and Techniques. He was a corecipient of the 2002 Best Student Paper Award (Second Prize) presented at the IEEE Radio Frequency Integrated Circuit (RFIC) Conference.

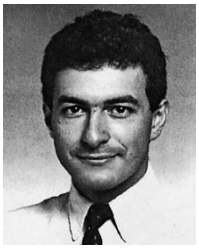

Gabriel M. Rebeiz (S'86–M'88–SM'93–F'97) received the Ph.D. degree in electrical engineering from the California Institute of Technology, Pasadena, in 1988.

In September 1988, he joined the faculty of The University of Michigan at Ann Arbor, and was promoted to Full Professor in 1998. He held short visiting professorships with the Chalmers University of Technology, Göteborg, Sweden, Ecole Normale Superieur, Paris, France, and Tohoku University, Sendai, Japan. His research interests include applying micromachining techniques and MEMS for the development of novel components and subsystems for radars and wireless systems. He is also interested in Si/GaAs RF integrated circuit (RFIC) design for receiver applications, and in the development of planar antennas and microwave/millimeter-wave front-end electronics for communication systems, automotive collision-avoidance sensors, monopulse tracking systems, and phased arrays.

Prof. Rebeiz was the recipient of the 1991 National Science Foundation Presidential Young Investigator Award and the 1993 URSI International Isaac Koga Gold Medal Award for Outstanding International Research. He was also the recipient of the 1995 Research Excellence Award presented by The University of Michigan at Ann Arbor. Together with his students, he was the recipient of Student Paper Awards at the IEEE Microwave Theory and Techniques Symposium (1992, 1999–1994), the IEEE Radio Frequency Integrated Circuits Symposium (RFIC) (2002), and the IEEE Antennas and Propagation Symposium (1992, 1995). He was also the recipient of the 1990 *Journées Int. de Nice sur les Antennes* (*JINA*) Best Paper Award. He was selected by his students as the 1997–1998 Eta Kappa Nu EECS Professor of the Year. He was also the recipient of the 1998 College of Engineering Teaching Award and the 1998 Amoco Foundation Teaching Award, given yearly to one faculty member of The University of Michigan at Ann Arbor for excellence in undergraduate teaching. He was the corecipient of the IEEE 2000 Microwave Prize for his work on MEMS phase shifters.